

POSITIONING PERFORMANCE ANALYSIS OF HIGH-ORDER BOC SIGNALS IN ADVANCED MULTI-CONSTELLATION HIGH-SENSITIVITY GNSS RECEIVERS

Sergi Locubiche-Serra⁽¹⁾, David Gómez-Casco⁽¹⁾, Adrià Gusi-Amigó⁽²⁾,
José A. López-Salcedo⁽¹⁾, Gonzalo Seco-Granados⁽¹⁾, José A. García-Molina⁽³⁾

⁽¹⁾ *Universitat Autònoma de Barcelona (UAB), IEEC-CERES, Spain*

Email: {sergi.locubiche, david.gomez.casco, jose.salcedo, gonzalo.seco}@uab.cat

⁽²⁾ *Vitrociset Belgium for European Space Agency (ESA/ESTEC), The Netherlands*

Email: a.gusiamigo@vitrocisetbelgium.com

⁽³⁾ *HE Space for European Space Agency (ESA/ESTEC), The Netherlands*

Email: jose.antonio.garcia.molina@esa.int

ABSTRACT

This paper addresses the problem of false locks that high-order BOC signals are prone to suffer from. To do this task, a multi-constellation high-sensitivity GNSS receiver is implemented so as to simultaneously use BPSK, low- and high-order BOC signals. The design of the receiver stages, mainly acquisition, tracking and PVT (position, velocity, time), is widely described. Several techniques, such as the bump jumping, double optimization multi-correlator-based and BPSK-like techniques are introduced at the tracking stage to circumvent the problem of false locks. Results are provided to compare the performance of these techniques at PVT level, unveiling the impact of false locks in terms of positioning error. These results allow us to conclude on the outperforming technique to mitigate false locks in practical environments.

1. INTRODUCTION

With the upcoming full operability of the Galileo system, the trend of next-generation Global Navigation Satellite System (GNSS) receivers moves towards providing positioning services using multiple constellations simultaneously, such as GPS, Galileo or Glonass [1]. In addition, these constellations are implementing high-order BOC signals, which provide a significant enhancement in terms of positioning accuracy with respect to conventional BPSK signals. This improvement is owing to the increase of the Gabor bandwidth, which leads to a reduction of the Cramér-Rao bound of the code-delay estimates [2, 3].

However, high-order BOC signals present several disadvantages. The most important drawback is the presence of secondary lobes in the autocorrelation function that are very little apart from each other and whose amplitude is very similar to the main correlation peak. This causes the cross-ambiguity function (CAF) of high-order BOC signals to be ambiguous due to the

difficulties to distinguish the main correlation peak, particularly in scenarios with low carrier-to-noise ratio (C/N_0) such as deep urban canyons. The acquisition of a secondary peak leads to an incorrect estimation of the code delay, introducing a bias of some meters in the user's position [4].

Different papers in the literature have focused on circumventing this ambiguity at the receiver's acquisition [5] or tracking stages at signal level. In the latter, examples of techniques for false-lock mitigation are the bump-jumping (BP) [6], double estimation technique (DET) [7], double optimization multi-correlator-based estimator (DOME) [8, 9] and full-BPSK methods [10]. Nevertheless, less attention has been paid to the analysis of this phenomenon in terms of user positioning.

Therefore, the objective of this work is to bring to the reader some insight into the impact of false locks of high-order BOC signals and compare the performance of false-lock mitigation techniques at positioning level. To this end, we have implemented an advanced high-sensitivity software GNSS receiver to deal with multi-constellation signals with different modulations such as BPSK and low- and high-order BOC. In this work, we also provide a wide description of the advanced features of our software receiver in each of its stages.

2. HIGH-SENSITIVITY GNSS RECEIVER

This section describes the GNSS software receiver designed in this work. The GNSS receiver consists in three stages: acquisition, tracking and PVT (positioning, velocity, time).

2.1. Acquisition

The first stage of the GNSS receiver is the acquisition of satellites. The objective of this stage focuses on the detection of the received signals from different satellites in view and provides a coarse estimation of Doppler

frequency and code delay.

This process is usually performed by computing the CAF for each satellite. The CAF consists in correlating the received signal with a local replica of the signal broadcasted from the satellite evaluating several trial values of frequency offset and code delay. The CAF can be expressed as a scaled version of the autocorrelation function,

$$R_p(\Delta\tau, \Delta f) = A_p e^{j\theta_p} \text{sinc}(\Delta f T_{coh}) r(\Delta\tau) + \omega, \quad (1)$$

where A_p is the amplitude obtained from the CAF with phase θ_p of the p th satellite, Δf is the frequency offset between the received signal and the local replica, $\Delta\tau$ is the code-delay offset, T_{coh} is the coherent integration time, and $r(\Delta\tau)$ is the autocorrelation function of a high-order BOC signal. The sinc term captures the degradation of the CAF owing to the frequency offset.

An example of an ideal CAF of a BOC(15, 2.5), as a representative case of high-order BOC signals, is illustrated in Figure 1, without considering noise effects. In the code-delay domain, it presents 25 peaks, but only the main peak allows the receiver to estimate accurately the user's position. The rest of the peaks offer a biased estimation of the user's position. For this reason, the problem of solving the ambiguity introduced by high-order BOC autocorrelation is of paramount importance, which is analyzed in more detail at the tracking stage.

Furthermore, although the CAF usually permits us to detect the presence of satellites in reasonably high C/N_0 conditions, it is not enough to acquire satellites in indoor or urban environments. This occurs because the signal suffers from a strong degradation owing to the obstacles of the channels in these environments [11]. The optimal way to obtain a gain in terms of signal detection is using a longer T_{coh} to compute the CAF. Nonetheless, the T_{coh} duration is limited in practice because of some impairments such as frequency offsets, phase noise and the presence of data bits.

To circumvent these limitations and be able to obtain some benefits in terms of signal acquisition, we must resort to the use of post-detection integration (PDI) techniques. These techniques allow the receiver to perform a more reliable decision about the presence of the satellites by combining different CAFs non-linearly. To carry out this task, our receiver includes two PDI techniques: the non-coherent PDI (NPDI) and differential PDI (DPDI) technique, which are defined as,

$$Z_{NPDI} = \sum_{n=1}^{N_{nc}} |R_{p,n}(\Delta\tau, \Delta f)|^2, \quad (2)$$

$$Z_{DPDI} = \left| \sum_{n=2}^{N_{nc}} R_{p,n}(\Delta\tau, \Delta f) R_{p,n-1}^*(\Delta\tau, \Delta f) \right|, \quad (3)$$

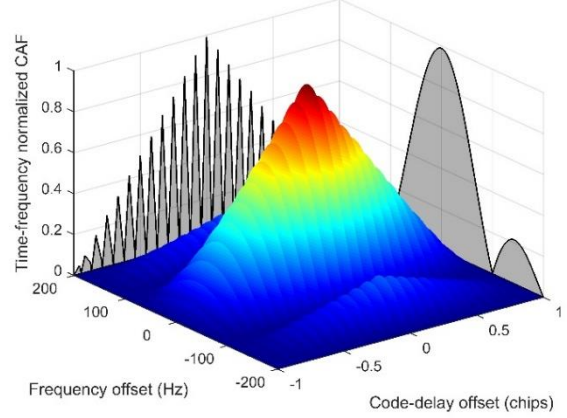


Figure 1. Ideal CAF of a BOC(15, 2.5) signal.

where $n = 1, \dots, N_{nc}$ indicates the time instant where the CAF is computed, and N_{nc} is the number of non-coherent combinations. The NPDI is the most common technique implemented in high-sensitivity GNSS receivers to detect weak signals. It removes the impairments that limit the T_{coh} duration by combining N_{nc} consecutive CAFs using the squared absolute value. The other alternative is the DPDI technique, which offers a better performance than NPDI technique in the absence of data bits. The fundamental aspect of the DPDI technique is that the signal components of two consecutive CAFs are highly correlated, while the noise components are completely uncorrelated.

An illustrative comparative between the NPDI and DPDI techniques is shown in Figure 2 in terms of their receiver operating characteristic (ROC) curves. As can be observed, the NPDI is insensitive to the presence of data bits, whereas the DPDI is highly affected by bit transitions. An exhaustive performance comparative of the NPDI, DPDI, and other PDI techniques can be found in [12].

The detection of the satellites is carried out by the comparison of the maximum value of the metric Z_{NPDI} or Z_{DPDI} with a given detection threshold. If the maximum magnitude of this metric surpasses the threshold, the satellite is considered to be present and a coarse estimation of the code delay and frequency Doppler is provided. However, when this magnitude does not exceed the threshold, the satellite is assumed not to be present. Reference [4] includes more details about the definition of the detection threshold. This process is performed for all possible satellites in view and when the receiver has acquired some of these satellites, the tracking stage is then started.

2.2. Tracking

The problem of false locks in high-order BOC signals has been addressed in the literature by some authors

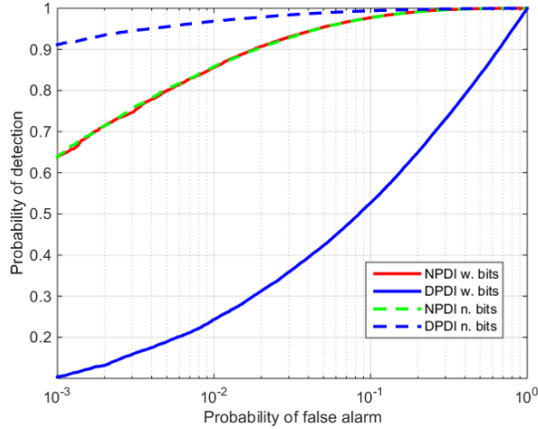


Figure 2. Example of ROC curves for NPDI and DPDI with $C/N_0 = 20$ dB-Hz, $T_{coh} = 100$ ms, $N_{nc} = 20$.

at tracking level, or in terms of closed-loop processing. The techniques can be divided into closed-loop and open-loop techniques.

2.2.1. Closed-loop techniques

BPSK-like methods are one type of solution for the problem at hand [13]. The equivalent BPSK envelope of one sub-carrier, or a combination of both sub-carriers, can be used to unambiguously track the signal. This can be observed in Figure 3, where the equivalent BPSK envelope given by the striped plot is used as the local replica to distinguish the main peak. The cost of this kind of methods is an accuracy degradation with respect to the original BOC signal. The reason is two-fold. On one hand, the Gabor bandwidth suffers from a drastic reduction when down-converting the signal. On the other hand, the signal power suffers from a 3-dB loss when retaining only one of the BOC subcarriers.

Other techniques aim at tracking the main lobe of the original BOC signal, and hence, attaining the corresponding high accuracy. In general, they are designed in a way to detect and subsequently correct a false lock. The first proposed solution for this family of techniques is the Bump Jumping [14]. The approach of this technique is to compare the energy at the adjacent lobes to the main lobe during the tracking. This can be done by placing two extra correlators, the very early (VE) and very late (VL) correlators, located at the corresponding distances in order to perform the energy comparison. The overall idea is that, if the energy at the VE or VL correlators is perceived as higher as the energy in the prompt correlator, the algorithm corrects the code estimation and jumps to the proper delay. In this work, an optimized version of the technique with respect to the conventional one found in the literature is used, which simply implements some non-coherent integrations to reduce the distortion of the correlation function.

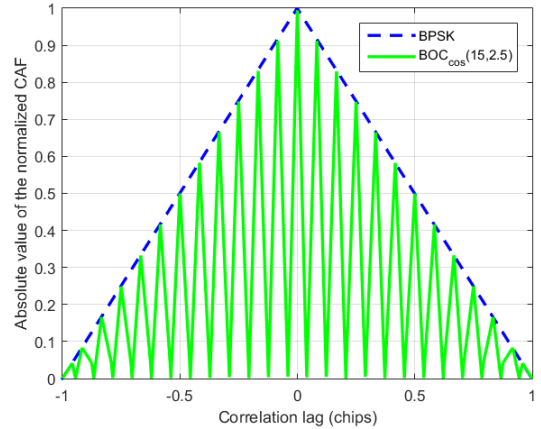


Figure 3. Example of autocorrelation function for a BOC(15, 2.5) signal versus equivalent BPSK envelope.

Another type of BOC-like techniques are the ones using two time-delay tracking loops, one for code; the Delayed Lock Loop (DLL), and one for the sub-carrier; the Sub-carrier Lock loop (SLL). This is the case of the Double Estimator [15] and Code-Subcarrier Smoothing [16] techniques. The false lock is detected and corrected with a certain combination of the output DLL and the SLL. All mentioned techniques require, in general, a low number of correlators.

2.2.2. Open-loop techniques

A different approach dealing with the false-lock issue is open-loop processing [2]. In open-loop, the signal is processed in batches of data and a set of parameters is estimated independently from each batch, similarly to the acquisition step. In order to reduce the parameter search complexity, some a-priori information regarding the parameters can be taken into account. Moreover, a larger number of observable correlators can be made available with respect to closed-loop processing. With a larger number of correlators, the main lobe and also some or all the side lobes can be observed.

In order to describe the open-loop techniques, let us define the multi-correlator receiver. Let us assume that K samples are taken from the cross-correlation function in (1) with the Doppler shift wiped off. The samples are denoted as k_n , with $n = 1, \dots, K$. Let us express the vector of K cross-correlation samples as,

$$\mathbf{x}_i = (x_{i,1} \cdots x_{i,K})^T = (R_p[k_1] \cdots R_p[k_K])^T \quad (4)$$

where \mathbf{x}_i is the complex correlation vector at instant i and $R_p[k] = R_p(kT_s)$ is the discrete cross-correlation signal with the Doppler shift wiped off and sampled at a sampling frequency $f_s = 1/T_s$. The negative log-likelihood function of the time delay τ and received complex amplitude β_p can be written as,

$$\Delta(\tau, \beta_p) = (\mathbf{x}_i - \beta_p \mathbf{r}(\tau))^H \boldsymbol{\Sigma}^{-1} (\mathbf{x}_i - \beta_p \mathbf{r}(\tau)), \quad (5)$$

where β_p encompasses the residuals of the code delay and frequency offset, and $\boldsymbol{\Sigma}$ is the noise covariance matrix, which can be computed with values from the vector of autocorrelation samples $\mathbf{r}(\tau)$ [2], defined as,

$$\mathbf{r}(\tau) = (r(k_1 T_s - \tau) \cdots r[k_K T_s - \tau])^T. \quad (6)$$

Post-correlation ML estimation

Once we know the distribution of the correlators outputs, we can perform a maximum likelihood (ML) estimation of the time delay with the post-correlation samples, that is, finding the model that fits better with the data, taking the distribution of the data into account. The ML estimate of β_p can be written as,

$$\hat{\beta}_{p,i} = (\mathbf{r}(\tau)^T \boldsymbol{\Sigma}^{-1} \mathbf{r}(\tau))^{-1} \mathbf{r}(\tau)^T \boldsymbol{\Sigma}^{-1} \mathbf{x}_i. \quad (7)$$

The maximum likelihood estimation of τ with N accumulated signals can be expressed as,

$$\hat{\tau} = \arg \min_{\tau} f(\tau)$$

$$f(\tau) = \sum_{j=0}^{N-1} (\mathbf{x}_{i-j} - \hat{\beta}_{p,i-j} \mathbf{r}(\tau))^H \boldsymbol{\Sigma}^{-1} (\mathbf{x}_{i-j} - \hat{\beta}_{p,i-j} \mathbf{r}(\tau)) \quad (8)$$

Note that this technique can be applied in a classic 3 correlator scheme upon considering that the complex correlator vector is as,

$$\mathbf{x}_i = (x_{i,1} \ x_{i,2} \ x_{i,3})^T = (R_p[k_1] \ R_p[k_2] \ R_p[k_K])^T \quad (9)$$

where $x_{i,1}$, $x_{i,2}$ and $x_{i,3}$ refer to the early, prompt, and late correlators, respectively. In the context of a receiver operating in tracking mode with a DLL, the technique can be employed in the following way. The estimator in (8), with signal integrations or not, can be used as a discriminator in order to obtain the code error information. The code error can then be provided to the code tracking loop.

Non-coherent/Differential integrations

Another option is to accumulate directly the correlation vectors using non-coherent integrations. The resulting accumulated signal vector can be expressed as,

$$\mathbf{z}_i = (z_{i,1} \ z_{i,2} \ z_{i,3})^T \quad (10)$$

where each element $z_{i,k}$ of the vector can be computed non-coherently as in (2),

$$z_{i,k} = \sum_{j=0}^{N-1} |x_{i-j,k}|^2 \quad (11)$$

where N is the number of integrations. Upon performing this operation, the sensitivity of the receiver can be increased [17]. The number of integrations is set taken into account the trade-off between the gain in sensitivity and the loss due to dynamic stress. The integration can be performed with the differential method as seen in (3),

$$z_{i,k} = \left| \sum_{j=0}^{N-2} x_{i-j,k} x_{i-j-1,k}^* \right|. \quad (12)$$

2.3. PVT

The PVT module of a GNSS receiver is responsible for ultimately providing the navigation and timing solutions (i.e. user position) using the measurements of code delay and Doppler shift coming from the tracking stage. The PVT module developed in this work is particularly designed with a three-fold perspective. Firstly, it is prepared to work in the high-sensitivity region (i.e. low C/N_0). Secondly, it is designed to maximize the positioning service availability. Thirdly, it combines BPSK, low- and high-order BOC signals and a weighted least squares approach with some initial values in order to maximize the positioning accuracy. To this end, some advanced features with respect to conventional GNSS receivers have been implemented.

2.3.1. Non-decoding of navigation message

The PVT module designed in this work presents the ability to provide a PVT solution without decoding the navigation message from the received signals. This makes the receiver suitable for the high-sensitivity region, where the C/N_0 is too low to decode the navigation message. This also presents the advantage of not having to wait for at least 30 seconds to decode the first navigation message and start providing a solution. On the counterpart, the Time-Of-Week (TOW), or the transmit time at which the messages leave the satellites, must be estimated at user level (i.e. as part of the navigation solution). Some authors refer to this problem in the literature as coarse-time navigation [18-20]. The drawback is that the initial value for the TOW must be in the region of the real value, for the least squares to converge to the correct solution. Even so, this drawback can be easily circumvented by the use of assisted data. Estimating the TOW requires computing the pseudoranges and pseudorange rates. To this end, the measurements coming from the tracking stage are used. Estimating pseudoranges requires solving the integer millisecond ambiguity, finding the solution that satisfies all satellites simultaneously. The rationale is that the code delay provided by tracking refers to a fractional

pseudorange, that is, the delay inside a code period, but the information about the integer millisecond part is missing. The process of solving the integer millisecond ambiguity is explained in detail in [18], along with an explanation on how to solve integer roll-overs.

The process of computing pseudorange rates is summarized in calculating the radial velocity of satellites (i.e. the parameter that origins coarse-time errors) using the Doppler shift as,

$$v_p = \frac{f_{shift}}{f_0} c \quad (13)$$

where f_{shift} is the Doppler shift, f_0 is the carrier frequency, and c is the speed of light.

2.3.2. Hybridization of multiconstellation measurements

The PVT module designed in this work is also prepared to provide a PVT solution combining measurements from different GNSS constellations. The main advantage is a significant enhancement of the service availability, since the receiver is now taking benefit from an increased number of useful satellites.

On the counterpart, one has to keep in mind that the measurements coming from different constellations may not be referred to the same time reference. That is, there may exist some time offset among the system clocks of different constellations. This is real, for instance, between GPS and Galileo constellations, which use respectively the GPS time (GPST) and the Galileo system time (GST) [21, 22]. The time offset for this particular case is the so-called GPS to Galileo Time Offset (GGTO).

In practice, this information is usually comprised in the navigation messages, which in this work are not decoded. Hence, the solution adopted in this section is to estimate the clock offset among different systems, denoted herein as Δt_{GNSS} , so as not to degrade the PVT solution in the order of some meters [23]. Similarly to Section 2.3.1, this is carried out at user level. Therefore, the number of unknowns to be solved as part of the navigation solution is increased by one.

2.3.3. Hybridization with high-order BOC signals

The most interesting feature of the PVT module designed herein is the ability to combine measurements of BPSK and low-order BOC signals with high-order BOC signals. This opens thus the door to high-accuracy positioning capabilities thanks to the latter group.

For this to work, we introduce an additional time offset, in the understanding that the nature of high-order BOC signals is different from BPSK or low-order BOC signals. Therefore, it is realistic and reasonable to think that high-order BOC signals may present a different

clock offset, denoted herein as Δt_{HBOC} . It can be understood as an additional Δt_{GNSS} between high-order BOC signals and the reference system clock.

The aim of the feature presented in this section is to estimate such time offset, also at user level, in an identical way to Section 2.3.2. Therefore, the number of unknowns is increased by one more.

2.3.4. Weighted Least Squares

To the end of providing navigation and timing solutions, a least squares approach with some initial values is usually adopted in conventional GNSS receivers. Let us define the system to be solved as,

$$\Delta \rho = \mathbf{H} \cdot \Delta \mathbf{x} \quad (14)$$

where $\Delta \rho$ is a column vector containing the pseudorange residuals for all satellites, \mathbf{H} is the so-called observation matrix, and $\Delta \mathbf{x}$ is a column vector containing the errors of the parameters that are being estimated as part of the navigation solution. For better understanding, the contents of these parameters are explained in detail in Section 2.3.5 for the PVT module under study. From (14), the least squares solution is given by [24],

$$\Delta \mathbf{x} = (\mathbf{H}^T \mathbf{H})^{-1} \mathbf{H}^T \cdot \Delta \rho \quad (15)$$

and the algorithm is run for a few number of iterations to ensure the convergence to the eventual solution and the minimization of the errors in $\Delta \mathbf{x}$.

Nonetheless, the PVT module designed in this work implements a more convenient approach, the so-called Weighted Least Squares (WLS), where a weighting matrix \mathbf{W} is introduced into the solution in (15) in order to take the quality of the different measurements into account and emphasize the contributions of those data samples that are deemed to be more reliable [24]. With this, for the WLS the solution in (15) turns into,

$$\Delta \mathbf{x} = (\mathbf{H}^T \mathbf{W} \mathbf{H})^{-1} \mathbf{H}^T \mathbf{W} \cdot \Delta \rho \quad (16)$$

with $\mathbf{W} \doteq \text{diag}([\sigma_1^{-2} \ \sigma_2^{-2} \ \dots \ \sigma_{\#SV}^{-2}]^T)$ a diagonal matrix containing the weights of the different satellites, given by σ_p^{-2} , where p refers to the p th satellite.

Many ways of computing the weights σ_p^{-2} can be found in the literature. The most common approach is based on the measured C/N_0 as a global indicator of the signal quality [25], also contemplating ionospheric perturbations [26]. Other references such as [27] base the weights on the elevation angle of the satellites, as a measurement related to multipath and tropospheric errors; the lower the elevation angle, the worse the measurements are prone to be.

In view of this, it would be of great interest to dispose of a metric to compute weights based on a combination of the two criteria above. Fortunately, an expression in

this regard can be found in the literature [27],

$$\sigma_p^{-2} = \frac{(\sin \theta_p)^2}{10^{-\left(\frac{C/N_{0p}(\text{dB})}{10}\right)}} \quad (17)$$

where θ_p is the elevation angle of the p th satellite. Expression (17) is thus the criterion used herein to compute the weights of the satellites for the WLS.

2.3.5. Navigation solution

With the features introduced throughout Section 2.3, and recalling (14), the minimum system to be solved turns out to be,

$$\begin{bmatrix} \Delta\rho_1 \\ \Delta\rho_2 \\ \Delta\rho_3 \\ \Delta\rho_4 \\ \Delta\rho_5 \\ \Delta\rho_6 \\ \Delta\rho_7 \end{bmatrix} = \begin{bmatrix} a_{x_1} & a_{y_1} & a_{z_1} & 1 & v_1 & \phi_1 & \varphi_1 \\ a_{x_2} & a_{y_2} & a_{z_2} & 1 & v_2 & \phi_2 & \varphi_2 \\ a_{x_3} & a_{y_3} & a_{z_3} & 1 & v_3 & \phi_3 & \varphi_3 \\ a_{x_4} & a_{y_4} & a_{z_4} & 1 & v_4 & \phi_4 & \varphi_4 \\ a_{x_5} & a_{y_5} & a_{z_5} & 1 & v_5 & \phi_5 & \varphi_5 \\ a_{x_6} & a_{y_6} & a_{z_6} & 1 & v_6 & \phi_6 & \varphi_6 \\ a_{x_7} & a_{y_7} & a_{z_7} & 1 & v_7 & \phi_7 & \varphi_7 \end{bmatrix} \begin{bmatrix} \Delta x_u \\ \Delta y_u \\ \Delta z_u \\ c\Delta t_u \\ \Delta t_s \\ \Delta t_{GNSS} \\ \Delta t_{HBOC} \end{bmatrix} \quad (18)$$

where $\Delta\rho_p$ is the pseudorange residual for the p th satellite, v_p is the radial velocity of the p th satellite as shown in (13), ϕ_p is valued 1 if the p th satellite belongs to the reference constellation and 0 otherwise, and φ_p is valued 1 if the p th measurement comes from a high-order BOC signal and 0 if not. For convenience,

$$a_{x_p} \doteq \frac{x_p - \hat{x}_u}{|x_p - \hat{x}_u|} \quad (19)$$

where x_p is the position of the p th satellite and \hat{x}_u is the estimated user position, both along the x -axis in ECEF (Earth-Centered, Earth-Fixed) coordinates. This applies also to a_{y_p} and a_{z_p} .

The system in (18) stands out the main drawback of this PVT module as is, which is the need for measurements from 7 different satellites, whereas a conventional GNSS receiver would provide a PVT solution with 4 measurements. This indeed poses a serious problem in scenarios where the number of available satellites is scarce, such as in urban environments, and the service availability may therefore be compromised.

As a way to circumvent this limitation we propose an approach based on fixing the value of the estimated time offsets, in the understanding that these are, in principle, constant over time. That is, the time offsets are not estimated at all time epochs (if not possible), but their value can be fixed (based on previous estimates) for some time, so as to reduce the number of needed satellites to provide a PVT solution when the signal conditions are very bad.

This effect can be observed in Figure 4, which shows an example of the number of available satellites under mild- and deep-fading conditions. Whereas more than 7 satellites are available in the former, the number drops down to 4 in the latter, and some time offsets must be fixed so as not to interrupt the service. Even though this will induce some error in the positioning solution due to the fluctuations that the time offsets may present, it is still possible to provide a reasonable PVT solution using this approach. It is worth mentioning that, in an extreme situation, the number of satellites needed for PVT can be reduced to as few as 2 for a 2D positioning solution, and 3 for a 3D solution, thus maximizing the service availability in harsh environments.

3. PVT RESULTS

In this section some preliminary results at PVT level are provided, and the objective here is two-fold. Firstly, to see the impact of false locks in high-order BOC signals. Secondly, to evaluate how the tracking techniques presented in Section 2.2 perform in mitigating these errors. The results presented herein are based on a combination of BPSK and low-order BOC signals, plus one high-order BOC signal with the same propagation conditions as the former group.

3.1. PVT solution under mild-fading conditions

This section presents the results of a test based on scenarios with mild-fading conditions, with a nominal C/N_0 of 35 dB-Hz and fadings that cause the C/N_0 to decrease down to 20-25 dB-Hz. The results are shown in Figure 5 in terms of the RMSE of the 2D position (in latitude-longitude coordinates).

As can be observed, the impact of false locks is stood out by the full BOC technique, where the full BOC signal is used as the local replica with no further processing. The technique presents an RMSE of 11.58 meters and thus provides a biased user position. These errors owing to false locks are significantly mitigated when using the tracking techniques introduced in Section 2.2, which are particularly designed for this purpose, and provide an RMSE below 3 meters. The BPSK envelope presents an RMSE of 2.93 meters, and even though the technique mitigates false locks successfully, it presents some accuracy degradation due to the reduction of the Gabor bandwidth and the 3-dB loss. The optimized bump jumping can mitigate this effect, with an RMSE of 2.5 meters, but the technique that ultimately provides the lowest RMSE is the maximum likelihood estimator; it presents an RMSE of 2.34 meters, and thus improves the error of the full BOC by more than 9 meters and the one for the BPSK envelope by more than half a meter.

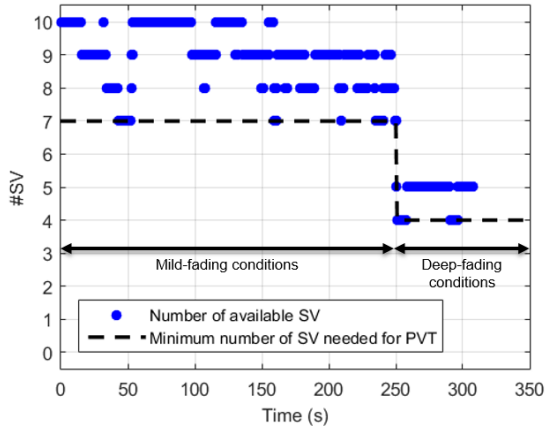


Figure 4. Ex. number of available SV versus minimum needed for PVT, mild- and deep-fading conditions.

3.2. PVT solution under deep-fading conditions

This section presents the results of a test based on scenarios with deep-fading conditions, with drops in the signal power causing the C/N_0 to go below 20 dB-Hz. The results are shown in Figure 5 in terms of the RMSE of the 2D position (in latitude-longitude coordinates). The results show that the full BOC technique is performing even better than in the mild-fading case, presenting an RMSE of 6.83 meters. This may be explained by the fact that the distortion of the correlation function and the secondary lobes may even facilitate the detection of the main peak. Even so, the solution provided by this technique is still biased with respect to the rest of techniques. For these, very similar conclusions to the mild-fading case can be extracted, where the main peak is tracked and thus their performance is very much alike, with an RMSE below 4 meters. The BPSK envelope and optimized bump-jumping techniques present an RMSE of 3.65 and 3.47 meters, respectively. Although by small difference, the technique of choice would be the maximum likelihood estimator, which presents an RMSE of 3.39 meters.

4. CONCLUSIONS

GNSS constellations are lately implementing the use of high-order BOC signals for accurate positioning services. In this work, the problem of false locks that this kind of signals is prone to suffer from has been addressed. To this end, a high-sensitivity software receiver has been designed to work at low C/N_0 and implements some advanced tracking techniques thought particularly for false lock mitigation. The performance of these techniques has been studied at PVT level, in terms of positioning error, as well as how false locks cause the navigation solution to be biased. Results show that the ML estimator is the most promising technique, outperforming the BPSK-envelope and bump-jumping

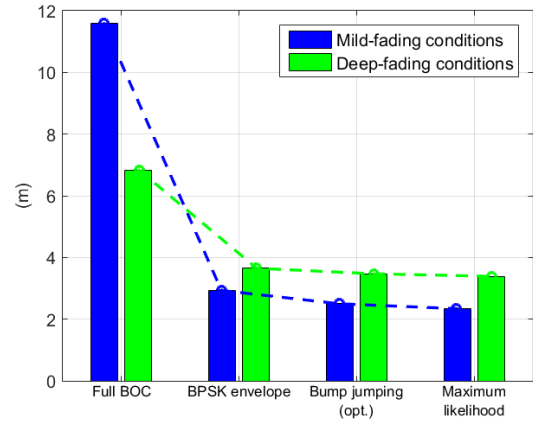


Figure 5. Techniques for false-lock mitigation. RMSE of 2D position under mild- and deep-fading conditions.

techniques in terms of positioning accuracy.

5. ACKNOWLEDGMENT

This work has been funded in part by the European Space Agency (ESA). The views presented in the paper represent solely the opinion of the authors and not necessarily the view of ESA.

6. REFERENCES

- Bonet, B., Alcantarilla, I., Flament, D., Rodriguez, C., & Zarraoa, N. (2009, September). The benefits of multi-constellation GNSS: reaching up even to single constellation GNSS users. In *Proceedings of the 22nd International Technical Meeting of The Satellite Division of the Institute of Navigation (ION GNSS)*, Savannah, GA, USA (pp. 22-25).
- Garcia-Molina, J. A., Navarro-Gallardo, M., Lopez-Risueño, G., Crisci, M. (2014). "Unambiguous tracking of high-order BOC signals in urban environments: Channel considerations". In *Proc. 7th Satellite Navigation Technologies and European Workshop on GNSS Signals and Signal Processing (NAVITEC)*, pp. 1-6.
- Borio, D. (2014). Double phase estimator: new unambiguous binary offset carrier tracking algorithm. *IET Radar, Sonar & Navigation*, 8(7), 729-741.
- Gomez-Casco, D., Lohan, E. S., Lopez-Salcedo, J. A., Seco-Granados, G. (2016). Multilag frequency estimation for high-order BOC signals in the acquisition stage. In *Proc. 8th. Satellite Navigation Technologies and European Workshop on GNSS Signals and Signal Processing (NAVITEC)* pp. 1-7.
- Gómez-Casco, D., Garcia-Molina, J. A., Gusi-Amigó, A., Crisci, M., López-Salcedo, J. A., & Seco-Granados, G. (2016, June). Mitigation of false locks

- in the acquisition of high-order BOC signals in HS-GNSS receivers. In *Localization and GNSS (ICL-GNSS)*, 2016 International Conference on (pp. 1-6). IEEE.
6. Fine, P., & Wilson, W. (1999). Tracking algorithm for GPS offset carrier signals. In *Institute of Navigation, National Technical Meeting 'Vision 2010: Present and Future'*, San Diego, CA (pp. 671-676).
 7. Hodgart, M. S., Blunt, P. D., & Unwin, M. (2008). Double estimator—A new receiver principle for tracking BOC signals. *Inside GNSS*, 3(3), 26-36.
 8. Garcia-Molina, J. A., Navarro-Gallardo, M., Lopez-Risueno, G., & Crisci, M. (2015, September). Robust unambiguous tracking of high-order BOC Signals: a multi-Correlator approach. In *ION GNSS* (pp. 1-6).
 9. Garcia-Molina, J. A., Navarro-Gallardo, M., Lopez-Risueño, G., & Crisci, M. (2016). Robust Unambiguous Estimation of High-Order BOC Signals: The DOME Approach. *Navigation*, 63(4), 511-520.
 10. Martin, N., Leblond, V., Guillotel, G., & Heiries, V. (2001, March). BOC (x, y) signal acquisition techniques and performances. In *Proceedings of the 16th International Technical Meeting of the Satellite Division of The Institute of Navigation (ION GPS/GNSS 2003)* (pp. 188-198).
 11. Seco-Granados, G., Lopez-Salcedo, J., Jimenez-Banos, D., & Lopez-Risueno, G. (2012). Challenges in indoor global navigation satellite systems: Unveiling its core features in signal processing. *IEEE Signal Processing Magazine*, 29(2), 108-131.
 12. Gómez-Casco, D., López-Salcedo, J. A., & Seco-Granados, G. (2016, June). Generalized integration techniques for high-sensitivity GNSS receivers affected by oscillator phase noise. In *Statistical Signal Processing Workshop (SSP)*, 2016 IEEE (pp. 1-5). IEEE.
 13. Burian, A., Lohan, E., and Renfors, M. (2006). BPSK-like methods for hybrid search acquisition of galileo signals. *IEEE International Conference on Communications ICC '06*, vol. 11, pp. 5211–5216.
 14. Fine, P., Wilson, W. (1999) Tracking algorithm for GPS offset carrier signals. *Proceedings of the 1999 National Technical Meeting of The Institute of Navigation*, January 25 - 27, San Diego, CA
 15. Hodgart, M. S., Blunt, P. D., and Unwin, M. (2007). The optimal dual estimate solution for robust tracking of binary offset carrier (BOC) modulation. In *Proceedings of the 20th International Technical Meeting of the Satellite Division of The Institute of Navigation (ION GNSS 2007)*.
 16. Navarro-Gallardo, M., López-Risueño, G., Crisci M., and Seco-Granados, G. (2012). Analysis of side lobes cancellation methods for BOCcos (n, m) signals. In *Satellite Navigation Technologies and European Workshop on GNSS Signals and Signal Processing*,(NAVITEC), 2012 6th ESA Workshop.
 17. Gusi, A., Closas, P., Garcia-Molina, J. A. (2016) False Lock Probability in BOC Signals. *Proceedings of the 2016 International Technical Meeting of the Satellite Division of The Institute of Navigation (ION GNSS 2016)*.
 18. Van Diggelen, F. S. T. (2009). *A-GPS: Assisted GPS, GNSS, and SBAS*. Artech House.
 19. Van Diggelen, F., & Abraham, C. (2007, September). Coarse-time AGPS; computing TOW from pseudorange measurements and the effect on HDOP. In *Proceedings of ION GNSS 20th international technical meeting of the satellite division, Fort Worth, TX, USA*.
 20. Petovello, M., & Muthuraman, K. (2012). GNSS Solutions: Coarse Time Positioning. *Inside GNSS*.
 21. Vanschoenbeek, I., Bonhoure, B., Boschetti, M., & Legenne, J. (2007). GNSS time offset: effects on GPS-Galileo interoperability performance. *Inside GNSS*, 2(6), 60-70.
 22. Hahn, J. H., & Powers, E. D. (2005, August). Implementation of the GPS to Galileo time offset (GGTO). In *Frequency Control Symposium and Exposition, 2005. Proceedings of the 2005 IEEE International* (pp. 5-pp). IEEE.
 23. Wang, J., Knight, N. L., & Lu, X. (2011). Impact of the GNSS time offsets on positioning reliability. *To appear in Journal of Global Positioning Systems*, 10(2).
 24. Kay, S. M. (1993). *Fundamentals of statistical signal processing: estimation theory*. Prentice Hall.
 25. Węzka, K. (2014). The Reliability Evaluation of GNSS Observations in the Presence of Ionospheric Perturbations. In *Mitigation of Ionospheric Threats to GNSS: an Appraisal of the Scientific and Technological Outputs of the TRANSMIT Project*. InTech.
 26. Kaplan, E., & Hegarty, C. (2005). *Understanding GPS: principles and applications*. Artech house.
 27. Tay, S., & Marais, J. (2013, December). Weighting models for GPS Pseudorange observations for land transportation in urban canyons. In *6th European Workshop on GNSS Signals and Signal Processing* (p. 4p).